A New Drop Weight Tensile Testing System for Soft Matter at Intermediate Strain Rates

Juan Carlos Nieto-Fuentes[1], Adeline Wihardja[2], Paul Stovall[2], Trent Wilson[2], Kaushik Bhattacharya*[2], and Daniel Rittel*[3]

[1]Department of Continuum Mechanics and Structural Analysis,
University Carlos III of Madrid, Av. de la Universidad, 30, 28911 Legans, Spain
[2]Division of Engineering and Applied Sciences,
California Institute of Technology, Pasadena CA 91125, USA
[3]Department of Mechanical Engineering,
Technion Israel Institute of Technology, 32000 Haifa, Israel

Abstract

This paper presents a novel and versatile tensile testing system based on the drop weight technique, specifically designed for materials that can undergo significant tensile deformation, such as elastomers. The core apparatus comprises of a hanging slender bar, from which a steel sleeve (referred to as the striker) is released under controlled conditions. Accelerated in free fall, the striker impacts a stationary plate, initially held in place by a mechanical detent. The specimen, secured by a gripping system between the hanging bar and the stationary support, undergoes controlled stretching at a nearly constant velocity upon the release of the detent triggered by the striker's impact. Full-field strain measurement is obtained using a high-speed camera in conjunction with digital image correlation. Additionally, strategically located piezoresistive force sensors enable real-time force measurements. By achieving strain rates ranging from 100 s^{-1} to 500 s^{-1}, this system addresses a notable gap in the literature concerning intermediate strain rate testing for soft materials.

1 Introduction

Tensile testing is a fundamental method used to evaluate the mechanical properties of materials, offering insights into strength, ductility, or elastic properties. It serves as a critical tool for researchers, engineers, and industries seeking to understand, improve, and ensure the performance and reliability of materials in various applications. The most common experimental device to characterize the tensile mechanical behavior of materials is the universal testing machine, either hydraulically or electromechanically driven. These apparatuses have proven for many years to be the workhorse of quasi-static experimentation, specifically in the range of strain rates from 10^{-4} s^{-1} up to 1 s^{-1}. At higher strain rates, ($\geq 10^3$ s^{-1} or "dynamic"), the Split Hopkinson Pressure Bar (SHPB) modified for tension [1, 2, 3, 4] or variations of the expanding ring testing technique [5, 6, 7, 8, 9] are extensively used to test a whole range of metallic or composite materials.

These techniques leave a gap in the realm of tensile testing at intermediate strain rates, from say ten to a few hundred per second. Quasistatic universal testing machines can not exceed tens

*Corresponding Authors. Email: bhatta@caltech.edu, merittel@technion.ac.il

per second, or do so at the expense of significant system vibrations, potentially affecting the load cell measurements (system ringing) thereby compromising the reliability of the test. Similarly, traditional Hopkinson bar systems cannot reach rates below 10^3 s^{-1}. This constraint arises from the duration of the loading pulse in a typical SHPB experiment, which is dependent on the length of the striker (specifically the pulse is twice the elastic wave travel time through the bar). One might consider increasing the loading time, but it necessitates a proportional increase in the length of the bars. This has been accomplished in a few facilities, like the ELSA Hoplab [10], but is not possible in a typical laboratory environment.

The SHPB also poses a number of challenges for soft materials such as elastomers: the large deformations these materials experience under tensile loading, the ability to reach stress equilibrium necessary to obtain the material response [11, 12], the detection of weak signals to measure forces due to impedance mismatch [13], or the application of a near constant strain rate during the test. A number of works in the literature have overcome these difficulties and successfully tested soft materials. For example, Nie *et al.* [3] tested EPDM rubber as a model material using a modified Split Hopkinson Tension Bar (SHTB), where cylindrical hollow bars were used instead of solid cross-section bars to minimize inertia effects, and force equilibrium was monitored by means of quartz crystal force transducers. Indeed, piezoelectric force transducers are widely used to increase the sensitivity of SHPB experiments when testing low-impedance and low-strength materials [14]. Another, more recent illustration is that of Upadhyay *et al.* [15] who use an innovative gripping method. Still, soft materials remains a challenge for SHPB.

In this work, we present a new and versatile, yet simple, tensile testing system based on the drop weight technique, capable of testing materials that experience large deformations under tension (soft materials like elastomers) at strain rates in the range $100\ s^{-1} - 500\ s^{-1}$. The device consists of a slender circular steel bar, on which a piece of steel tube (sleeve) is allowed to slide by gravity in free fall. The specimen is clamped between one end of the bar and at a standing plate which is being held by mechanical detents. Upon impact of the steel sleeve on the standing plate, the standing plate is released, causing the specimen to stretch uniaxially. The transient events and full-field strain measurements are recorded by means of a high-speed camera coupled with digital image correlation. Piezoresistive force sensors located on top of the bar allow for real-time force data acquisition. We present the system in Section 2, and demonstrate it with natural rubber in Section 3.

2 Experimental Method

2.1 Tensile drop tower design

The design of the tensile drop tower apparatus is based in the drop weight technique, a method commonly used for conducting compression tests at intermediate strain rates. In this study, we have adapted the same principle of a gravity-driven falling weight to conduct impact tests under tensile loading conditions. The apparatus can be basically divided into three parts: the top ensemble, the striker (driving force mechanism), and the bottom ensemble. The entirety of the setup is depicted in Figure 1, with details in Figure 2.

The top ensemble of the tensile drop tower, shown in Figure 2(a) consists of a stainless-steel slender bar with 31.75 mm of external diameter and a length of 1.8 m, suspended vertically from a steel plate. This plate is affixed to the laboratory ceiling via a series of rods, creating a 18 cm clearance between the plate and the ceiling. A precisely machined aperture in the plate allows the steel bar to pass through freely, enabling unimpeded vertical motion. To restrict vertical displacement during the experiment, while permitting slight rotational movement in the axial direction, an open

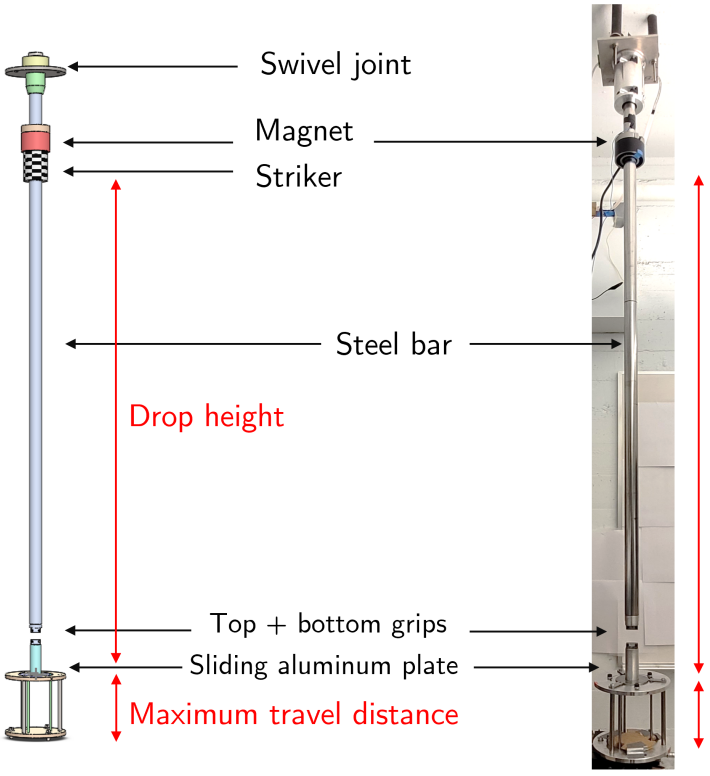

Figure 1: Schematic drawing (left) and image (right) of the drop weight tensile testing system. Note that the striker is not shown in the right image.

swivel joint is affixed to the end of the bar. On the opposite end of the stainless-steel bar, a gripping system comprised of two plates with knurled surfaces secures one side of the dog-bone specimen in place. Knurling of the grip plates surfaces is essential to prevent slippage of the specimen's shoulder during the experiment. Similarly, the other end of the specimen is clamped by a comparable grip system, situated on the lower base (bottom ensemble) of the drop tower apparatus.

As depicted in Figure 2(b), the bottom ensemble of the drop tower apparatus primarily comprises the following components: two aluminum plates (identified as items number 1 and 2) interconnected by three slender bars, a sliding aluminum plate (item 3) equipped with a restraint mechanism, an extension bar (item 4) housing the specimen grip system (item 5), and a crash pad (item 6) designed to absorb the impact from the striker. Item 1 can be readily affixed to either the laboratory floor or a robust bench, depending on the specific length requirements of the drop tower apparatus. In the case of this study, the aluminum plate is securely attached to a heavy-duty bench to ensure stability and reliability during experimentation. The aluminum plate designated as item 2 serves to secure the sliding plate (item 3) in position through the use of three ball-nose spring plungers. These locking mechanisms facilitate a stable alignment of the sliding plate before impact. Moreover, the detent mechanism's quick release, triggered by the impact force of the striker, minimizes kinetic energy loss, thereby optimizing the efficiency of the testing process. Smooth vertical motion of the sliding plate after-impact is facilitated by three linear shafts, in conjunction with linear bearings. This configuration ensures a seamless movement, contributing to the uniaxial stretch of the specimen during the test. The extension bar (item 4), anchored to the sliding plate

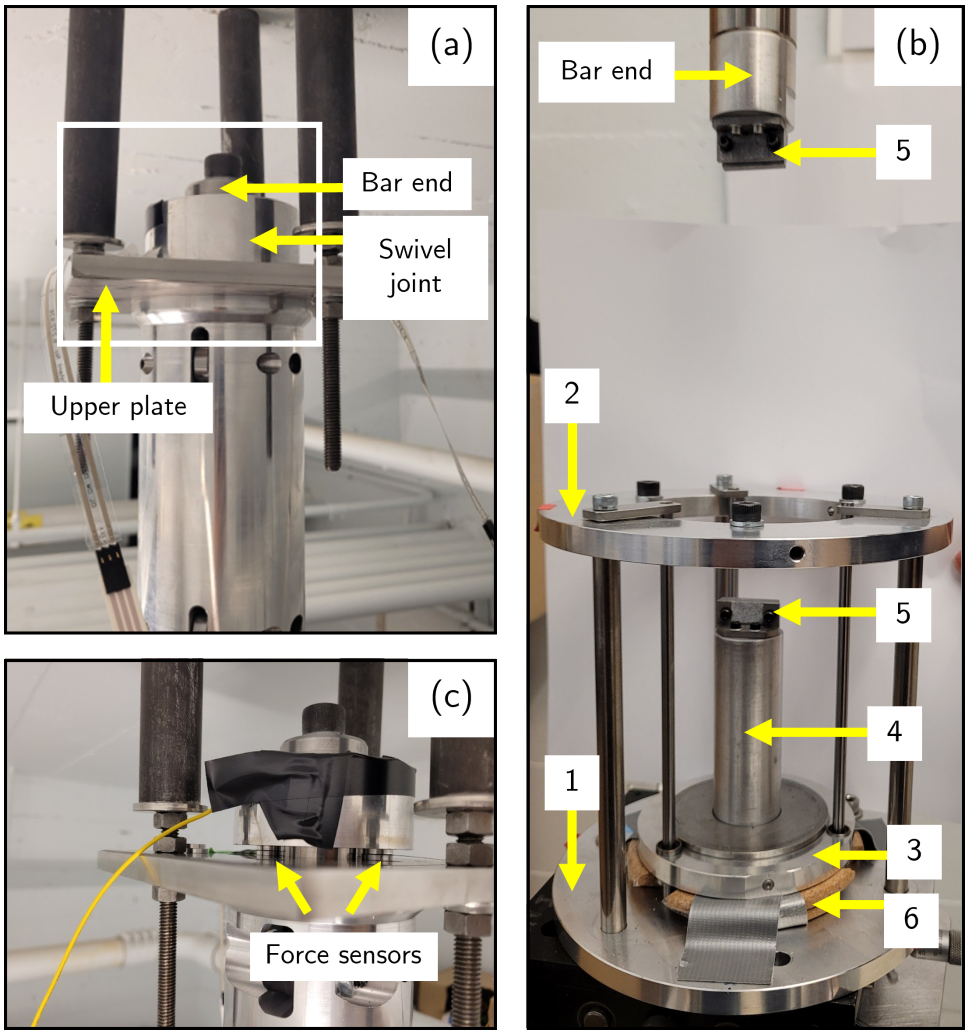

Figure 2: Details of the drop tower apparatus. (a) Top ensemble. (b) Bottom ensemble. (c) Force sensors placed in the top assembly of drop tower.

at one end and supporting the specimen's grip system at the other, measures 90 mm in length, mirroring the length of the striker to prevent obstruction of the specimen from the camera's field of view during testing. Maintaining coaxial alignment of the extension bar (that is, the bottom ensemble) with the hanging vertical bar (top ensemble) ensures that out-of-plane displacements on the specimen during testing are prevented.

The driving force for the experiment is provided by a steel sleeve, referred to as the striker, which features an internal diameter of 32 mm (coinciding to that of the bar, with a specific tolerance) and a thickness of 16 mm. The striker is securely held in place by a ring-shaped electromagnet, adjustable along the length of the hanging steel bar to meet the desired impact velocity for experimental needs. The release mechanism for the striker involves a normally-closed push button switch, offering a safe and controlled launch mechanism for the experiment. The sleeve has an internal Teflon (PTFE) bushing to facilitate a smooth sliding along the bar. The use of PTFE minimizes friction, allowing for effortless motion of the sleeve during the striker acceleration stage.

Noise in DIC measurements	
Strain (ϵ_{yy}), mean	5.4×10^{-5}
Strain (ϵ_{yy}), standard deviation	1×10^{-4}
Vertical displacement, mean	0.00022 mm
Vertical displacement, standard deviation	0.0003 mm

Table 1: Quantified DIC uncertainties from ten still images of the control sample.

2.2 Full field strain characterization

The experiments are captured using a high-speed full-field imaging technique. To achieve this, a Photron FASTCAM NOVA S12 high-speed camera equipped with a 100 mm Tokina AT-X Pro lens is synchronized with the striker release mechanism, enabling the collection of 5437 frames at 10000 frames per second with a resolution of 1024×1024 pixels. Throughout impact duration, a continuous light source (MultiLed LT) is used. The high-speed imaging setup is complemented by in situ 2D Digital Image Correlation (DIC), allowing for comprehensive analysis of displacement fields within the specimen. 2D DIC software (Vic2D, Correlated Solutions, Columbia, SC) was used to determine the full-field displacement of the specimen and the bottom plate. A black speckle pattern over a white background was used for correlation with a subset size of approximately 21×21 pixels and a step size of 1 pixel. The same parameters were used to determine the vertical velocity of the bottom plate, with a random speckle pattern applied to the bottom clamp holding the specimen.

Noise floor strain in DIC measurement is quantified by taking a series of ten still images of a control sample. Any displacement measured from these images via DIC is indicative of noise inherent in the imaging system, introducing error in our DIC. Under no deformation, the mean and standard deviation values of the full-field vertical displacement and strain are shown in Table 1. The highest displacement recorded was 0.0033 mm and the strain was 0.3%. Across a chosen set of control images, the intended zero strain is measured as strain on the order of 10^{-5}. False measurements due to the imaging setup are negligible.

2.3 Force measurement

Whereas strain gages are the most popular means to measure strains (quasi-static or even transient) in bars, their use is limited in the present setup by the fact that due to the pulse duration (several milliseconds), the "traditional" incident and reflected signals are due to overlap considerably, therefore precluding the straightforward determination of the applied load. To overcome this limitation, we opted for thin-film piezoresistive force (pressure) sensors in our design. These sensors offer rapid response times and high sensitivity, making them well-suited for capturing transient events typical of the intermediate strain rates encountered in drop tower testing. Specifically, we employed two Tekscan FlexiForce™A201 sensors, capable of measuring up (but not really limited) to 445 N in the standard range.

To ensure accurate force measurements, the sensors underwent conditioning and calibration procedures at room temperature before installation in the drop tower apparatus. Calibration involved the use of an MTS servohydraulic machine (Model 358.10) to apply loads within the expected force range, with the process repeated multiple times. The resulting calibration curve, shown in Figure 3, provides the relationship between the sensors' electrical output and actual force units. It is important to note that the sensor's sensing area measures 9.53 mm in diameter. To guarantee that the load is solely supported by this sensing area, the sensor is sandwiched between two thin aluminum discs of a diameter slightly smaller than the sensing area. This configuration ensures

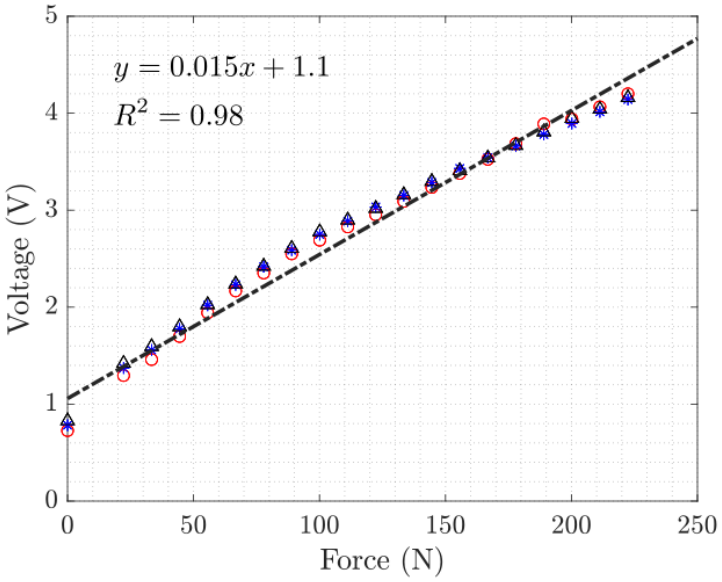

Figure 3: Calibration curve of the flexiforce sensors used to mesure force in drop tower experiments.

that the force applied is accurately detected by the sensor without interference from surrounding areas.

After calibration, the force sensors are positioned within the drop tower apparatus. Specifically, we have placed two diametrically opposed sensors, each sandwiched between the swivel joint on one end of the bar and the upper supporting plate, within the top assembly of the drop tower. A detailed view of this arrangement is provided in Figure 2(c). After the striker is launched, once the stress wave reach the force sensors, diagnostics are triggered at 200 MHz using a Siglent SDS 1202X-E digital oscilloscope to start recording force data.

There are noise-floor oscillations present in the force measurements, which generates uncertainty across all our experiments. We attribute such oscillations to various factors including electrical interference in the laboratory. Further, bending of the hanging steel rod and bending of the bottom plate as the striker travels downward will amplify these oscillations. To quantify the uncertainty in force measurements, we recorded the magnitude of oscillations at no load condition. Force oscillations of 7N on average are recorded; such oscillations are present throughout the entire testing duration.

3 Demonstration

Drop tower tests were carried out on six different samples of natural rubber (McMaster-Carr, 87145k411). Each sample is cut to be 30 mm $\times$ 10 mm and is 1.5 mm thick. In each test, the striker was dropped from a height of 0.75 m above the specimen that is clamped between the sliding plate and the stainless-steel bar, resulting in an impact velocity $v_{\text{impact}} = \sqrt{2gh} \approx 3.8$ m/s.

Figure 4 collects the observations of one particular test. Snap-shots of the deformation, and the resulting strain field across the specimen as captured by DIC, are shown in Figure 4(a). There is no noticeable cracking or removal of the speckles during DIC, and good correlation is maintained throughout the duration of impact, despite the large amount of strain produced by the specimen. Further, the strain field is uniform across the sample, and such uniformity is present across all

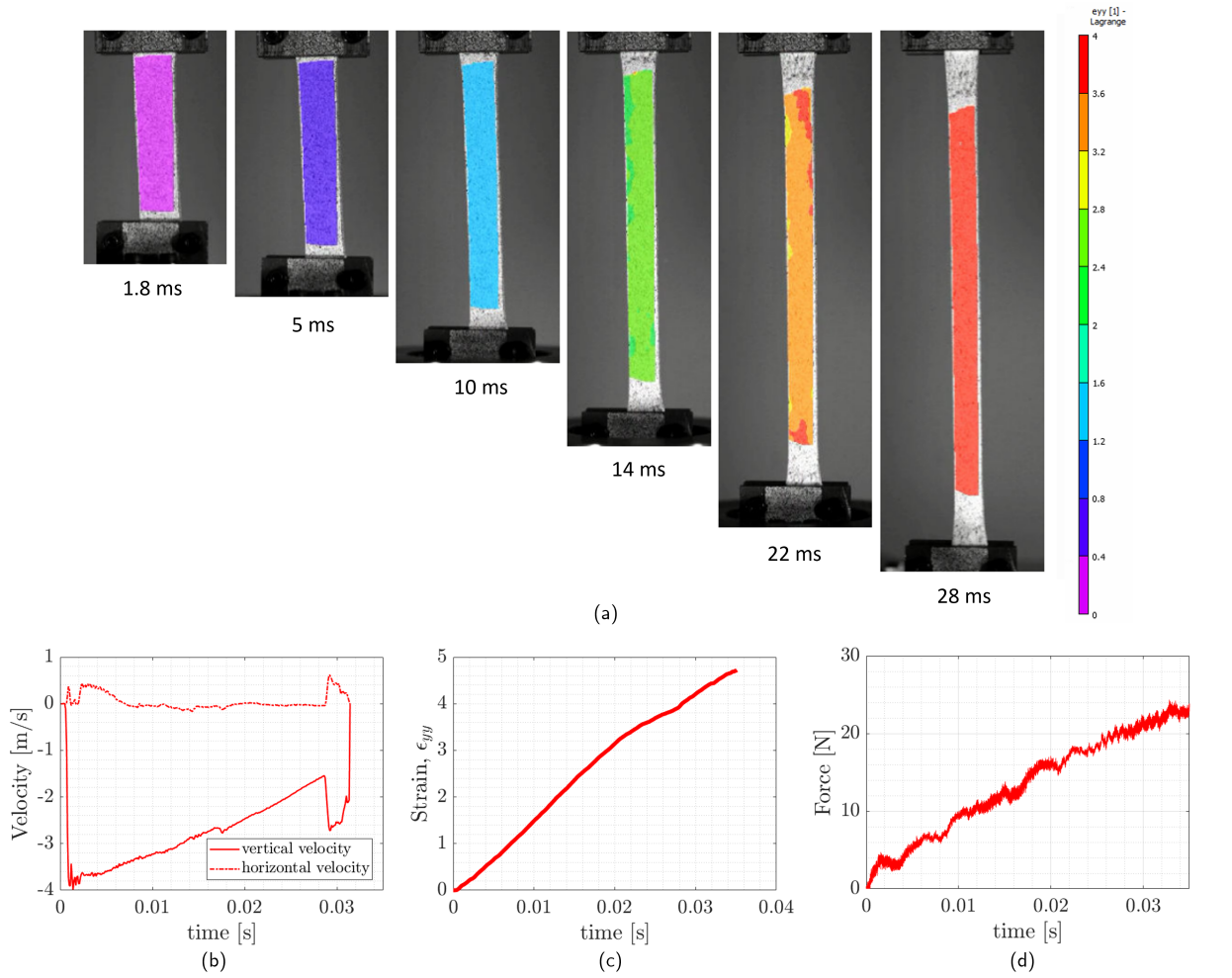

Figure 4: Representative experimental observations. Top: (a) Deformation of the specimen and the evolution of the strain fields as captured by DIC. Note that the strain is uniform across the sample. Bottom: (b) Vertical and horizontal velocity of the sliding plate from DIC analysis. (c) Strain in time from DIC analysis. (d) Force in time from force measurements.

samples tested. There is a significant extension of the specimen, but there is also some lateral motion of the bottom clamp due to the small tolerance between the striker and the sliding plate that holds the specimen. By adding a speckle pattern to the bottom clamp and using DIC, the velocity and displacement history of the bottom clamp is obtained; this is shown in Figure 4(b). The vertical velocity of 3.6 m/s at impact is consistent with the nominal impact velocity of 3.8 m/s. There is an initial small lateral displacement (1.5 mm at its peak), but this rapidly diminishes (after about 10 ms), and is extremely small compared to the vertical displacement. We obtain the strain in the sample from the DIC observations of the specimen, and the strain history is shown in Figure 4(c). Notice that the strain rate is relatively uniform. Finally, the average force exerted on the specimen is obtained via force sensors, as shown in Figure 4(d). Due to noise-floor already present in the force measurements, we filter our force measurements with a moving filter which uses a window size that averages high frequency oscillations, yet is small compared to the entire impact duration.

We now discuss the average behavior of all six natural rubber specimens tested. The resulting

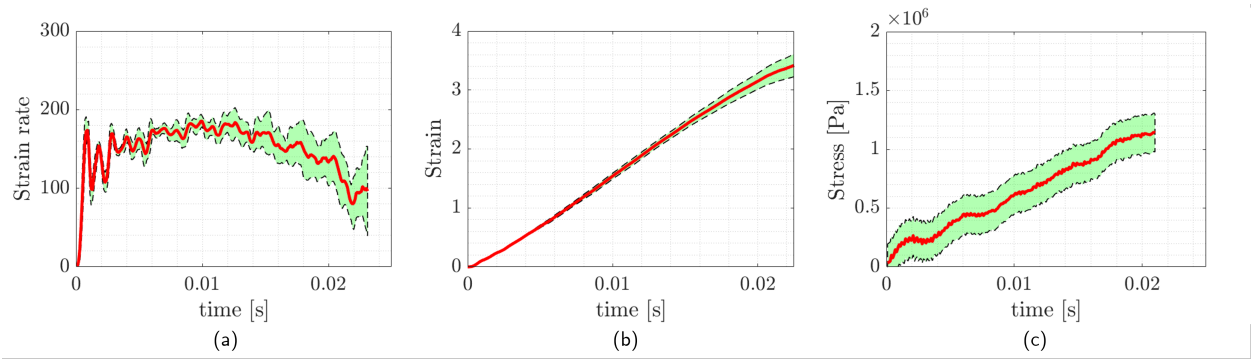

Figure 5: Drop tower results across six samples. (a) Average nominal strain rate of 155/s. (b) Strain in time. (c) PK stress in time; the upper and lower bound of stress are calculated from uncertainties in force measurements, as detailed in Section 2.3. Green envelopes represent experimental uncertainty.

strain rates in all six samples can be seen in Figure 5(a), in which the green envelope represents the spread of strain rates across all samples. Across all six samples, the nominal average strain rate achieved is 155/s. As illustrated, the specimen starts deforming at a constant strain rate immediately upon impact and maintains this value for approximately 20 ms. Afterwards, there is a gradual drop in strain rate, which DIC analysis indicates as slipping near the clamped region. This gradual drop is then followed by a sudden increase in strain rate that occurs from a second impact of the striker, as confirmed by DIC. This second impact occurs due to the striker bouncing from the sliding plate after the first impact, and then falling back to impact the sliding plate the second time. In post-processing, we neglect data gathered after 20 ms. The strain evolution with time can be seen in Figure 5(b), where again, the envelope represents the spread across all six samples. The average strain increases up to almost $\epsilon_{yy} = 4$ in 20 ms. Variations in loading conditions and in initial impact velocity contribute to variations of strain rates and strain across all specimens. We display the nominal or Piola-Kirchhoff or engineering stress (force with respect to the undeformed cross sectional area) history in Figure 5(c)). The Piola-Kirchhoff stress increases up to 1.2 MPa in 20 ms. The primary uncertainty in stress response is due to noise-floor oscillations in the force obtained from our force measurement system, as detailed in Section 2.3. This uncertainty is illustrated as the envelope in Figure 5(c)).

To verify our technique, we supplement our experimental observations with finite element simulations. We implement a Neo-Hookean constitutive model through deal.II finite element library [16]. We begin with the quasi-incompressible Neo-Hookean free energy of the form

$$W = \frac{\mu}{2}\left[J^{-2/3}\left(\lambda_1^2 + \lambda_2^2 + \lambda_3^2\right) - 3\right] + \frac{k}{2}(J-1)^2, \tag{1}$$

where $\lambda_1, \lambda_2, \lambda_3$ are the eigenvalues of the deformation gradient tensor, F, and $\lambda_1 \geq \lambda_2 \geq \lambda_3$. As usual, J is the determinant of F. We also add a viscous coontribution to the stress so that the Piola-Kirchhoff stress

$$S = \frac{\partial W}{\partial \nabla u} + J\left[\nu_1 \mathrm{Tr}(D) + \nu_2 \mathrm{dev}(D)\right] F^{-T}$$

where D is the rate of deformation, and ν_1 and ν_2 are the volumetric and deviatoric viscosity respectively. The parameters used in our simulations are listed in Table 2, and an impact velocity of 3.8 m/s is used. Further details can be found in Appendix A.

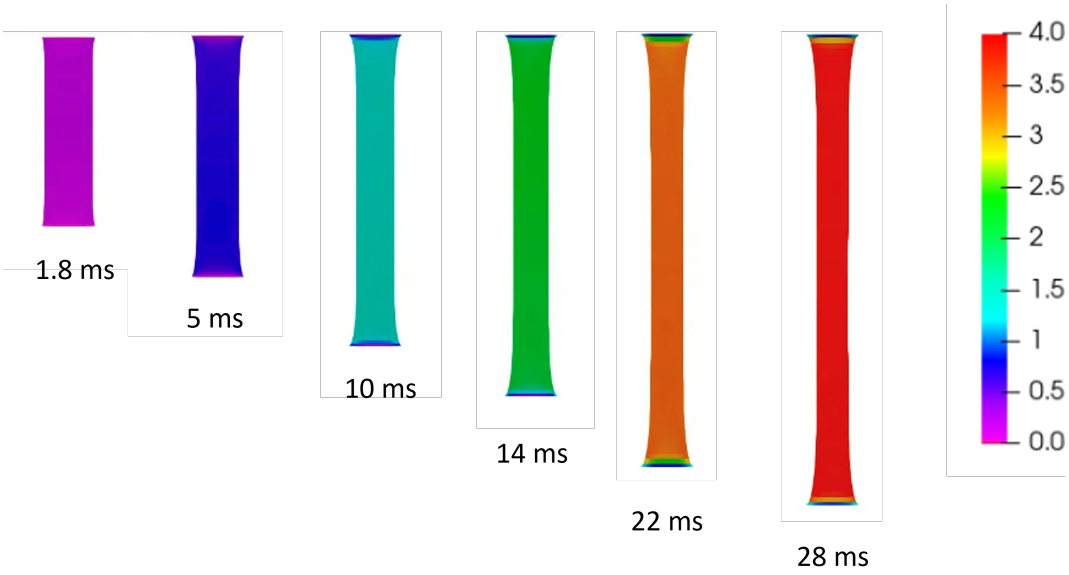

Figure 6: Time evolution of simulated strain fields. The strain fields are uniform across the sample.

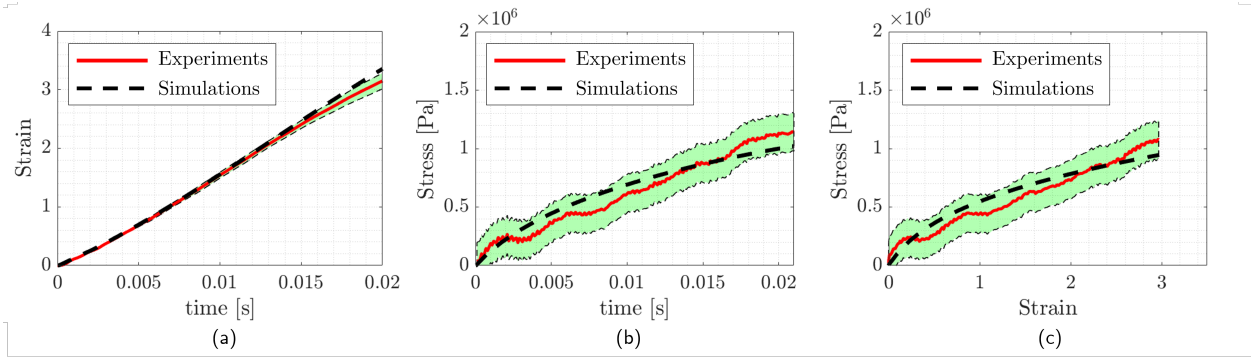

Figure 7: Comparison of simulation against drop tower experiments. (a) Strain in time. (b) PK stress in time. (c) Stress-strain in time. Green envelopes represent experimental uncertainty.

Parameters for numerical simulations	
Shear modulus μ	0.2×10^6 Pa
Poisson's ratio ν	0.49
Density ρ	1000 kg/m^3
Bulk viscosity, ν_1	150 Pa $\cdot$ s
Deviatoric viscosity, ν_2	20 Pa $\cdot$ s

Table 2: Parameters used for the numerical simulations of the drop tower experiments on natural rubber specimens to verify our experimental technique.

Figure 6 shows snaphots of the simulated deformation and strain field. The strain is again uniform. Comparing the simulated and the experimental deformation fields, we note that there is slipping in the experimental tests near the grips. Hence, the velocity of the sliding plate (used as boundary condition in our simulations) is higher than the actual velocity experienced by the specimen in our experiments. This slip, which is present across all samples tested, results in a higher perceived strain in the simulations (Figure 7(a)), especially closer to 20 ms. Nevertheless, there is a good agreement between experimental and simulated values. The observed experimental stress evolution and stress-strain curve is consistent with the simulated values (Figure 7(b), Figure 7(c)).

4 Conclusion

We have described a novel and versatile tensile testing system based on the drop weight technique, specifically designed for materials that can undergo significant tensile deformation, such as elastomers. The core apparatus comprises of a hanging slender bar, from which a steel sleeve (referred to as the striker) is released under controlled conditions. Accelerated in free fall, the striker impacts a stationary plate, initially held in place by mechanical detents. The specimen, secured by a gripping system between the hanging bar and the stationary support, undergoes controlled stretching at a nearly constant velocity upon the release of the detent triggered by the striker's impact. Full-field strain measurement is obtained using a high-speed camera in conjunction with digital image correlation. Additionally, strategically located piezoresistive force sensors enable real-time force measurements. By achieving strain rates ranging from 100 s^{-1} to 500 s^{-1}, this system addresses a notable gap in the literature concerning intermediate strain rate testing for soft materials.

This test system fills an important gap between universal testing machines that are typically limited to strain rates of 1 s^{-1} and below, and split-Hopkinson (Kolsky) pressure bars that is typically limited to strains of 10^3 s^{-1} and above. We have demonstrated the system with experiments in natural rubber with strain rates of 10^2 s^{-1} and strains of 3. In current and future work, we use the testing system to study the rate and history dependent properties of soft materials, including liquid crystal elastomers and biological materials, as well as architected materials.

Acknowledgement

We gratefully acknowledge the financial support of the National Science Foundation (DMS:2009289) and the Army Research Office (W911NF22-2-0120). J.C. Nieto-Fuentes acknowledges support from the CONEX-Plus programme funded by Universidad Carlos III de Madrid and the European Union's Horizon 2020 research and innovation programme, under the Marie Sklodowska-Curie grant agreement No. 801538.

A Computational approach

We implement this constitutive model to a dynamic setting through the incremental action integral

$$\mathcal{A} = \int_{t_1}^{t_2} \left[\left(\mathcal{E} - \int_\Omega f \cdot u \, d\Omega - \int_{\partial_t \Omega} t \cdot u \, dS \right) - \int_\Omega \rho \frac{\dot{u}^2}{2} \, d\Omega \right] dt, \tag{2}$$

where f and t are the body force and surface traction, respectively, and $\partial_t \Omega$ is the traction boundary. Here, the energy $\mathcal{E}$ is composed of our stored elastic energy density,

$$\mathcal{E} = \int_\Omega W(\nabla u, \Lambda, \Delta) \, d\Omega. \tag{3}$$

Stationarity of the action integral ($\delta \mathcal{A} = 0$) allows us to obtain equation of motion

$$0 = \int_\Omega \left(-\frac{\partial W}{\partial \nabla u} \cdot \nabla \varphi + f \cdot \varphi - \rho \ddot{u} \cdot \varphi \right) d\Omega + \int_{\partial_t \Omega} t \cdot \varphi \, dS \qquad \forall \varphi \in \mathcal{U}, \tag{4}$$

with $\mathcal{U} = \{u : u \in H^1(\Omega \times [0,T]), u = u_*(t) \quad \text{on } \partial_u \Omega\}$.

We consider discretization of the displacement field with bilinear quadrilateral, Lagrange finite element of degree 1. Thus, $u(x) = \sum_i u_i N_i(x)$, where u_i are the unknown expansion coefficients and $N_i(x)$ are the finite element shape functions, i.e., linear with compact support. The system is then solved by solving for displacement fields explicitly. We discretize equation (4) in the finite element space with central difference scheme in time, where we take $\ddot{u} = \frac{u^{n+1} - 2u^n + u^{n-1}}{\delta t^2}$. The resulting linear equation to be solved is thus $M_{ij} u_j^{n+1} = F_i^n$, with

$$M_{ij} = \int_\Omega \frac{\rho}{\Delta t^2} \, N_i(x) N_j(x) \, d\Omega, \tag{5}$$

$$F_i^n = \int_\Omega -\sigma(\nabla u^n, \Lambda^{n+1}, \Delta^{n+1}, u_*^{n+1}) \cdot \nabla N_i(x) + \rho \left(\frac{2u_j^n - u_j^{n-1}}{\Delta t^2} \right) \cdot N_i(x) \, d\Omega. \tag{6}$$

The integrals above are computed using Gauss quadrature formula.

References

[1] R. Gerlach, C. Kettenbeil, and N. Petrinic, "A new split hopkinson tensile bar design," *International Journal of Impact Engineering*, vol. 50, pp. 63–67, 12 2012.

[2] H. Huh, W. J. Kang, and S. S. Han, "A tension split hopkinson bar for investigating the dynamic behavior of sheet metals," *Experimental Mechanics*, vol. 42, pp. 8–17, 3 2002.

[3] X. Nie, B. Song, Y. Ge, W. W. Chen, and T. Weerasooriya, "Dynamic tensile testing of soft materials," *Experimental Mechanics*, vol. 49, pp. 451–458, 8 2009.

[4] B. Song, B. R. Antoun, K. Connelly, J. Korellis, and W. Y. Lu, "Improved kolsky tension bar for high-rate tensile characterization of materials," *Measurement Science and Technology*, vol. 22, 2011.

[5] J. Nieto-Fuentes, T. Virazels, N. Jacques, and J. Rodríguez-Martínez, "Gas gun driven dynamic expansion of 3d-printed alsi10mg rings," *International Journal of Impact Engineering*, vol. 180, p. 104556, 10 2023.

[6] J. Janiszewski and W. Pichola, "Development of electromagnetic ring expansion apparatus for high-strain-rate test," *Solid State Phenomena*, vol. 147-149, pp. 645–650, 1 2009.

[7] F. Gant, G. Seisson, P. Longère, S. E. Mai, and J.-L. Zinszner, "High strain rate responses of some metals and alloys using a plate impact driven ring expansion test (pidret)," *International Journal of Impact Engineering*, vol. 184, p. 104829, 2 2024.

[8] F. I. Niordson, "A unit for testing materials at high strain rates," *Experimental Mechanics*, vol. 5, pp. 29–32, 1965.

[9] H. Zhang and K. Ravi-Chandar, "On the dynamics of necking and fragmentation - i. real-time and post-mortem observations in al 6061-o," *International Journal of Fracture*, vol. 142, pp. 183–217, 2006.

[10] "European laboratory for structural assessment: Large hopkinson bar facility (elsa-hoplab)."

[11] D. Richler and D. Rittel, "On the testing of the dynamic mechanical properties of soft gelatins," *Experimental Mechanics*, vol. 54, pp. 805–815, 2014.

[12] B. Song and W. Chen, "Dynamic stress equilibration in split hopkinson pressure bar tests on soft materials," *Experimental Mechanics*, vol. 44, pp. 300–312, 6 2004.

[13] W. Chen, B. Zhang, and M. J. Forrestal, "A split hopkinson bar technique for low-impedance materials," *Experimental Mechanics*, vol. 39, pp. 81–85, 6 1999.

[14] W. Chen, F. Lu, and B. Zhou, "A quartz-crystal-embedded split hopkinson pressure bar for soft materials," *Experimental Mechanics*, vol. 40, pp. 1–6, 3 2000.

[15] K. Upadhyay, D. Spearot, and G. Subhash, "Validated tensile characterization of the strain rate dependence in soft materials," *International Journal of Impact Engineering*, vol. 156, p. 103949, 10 2021.

[16] D. Arndt, W. Bangerth, M. Feder, M. Fehling, R. Gassmöller, T. Heister, L. Heltai, M. Kronbichler, M. Maier, P. Munch, J.-P. Pelteret, S. Sticko, B. Turcksin, and D. Wells, "The `deal.II` library, version 9.4," *Journal of Numerical Mathematics*, vol. 30, no. 3, pp. 231–246, 2022.